Off-energy-shell p-p scattering at sub-Coulomb energies via the Trojan horse method

A. Tumino,[1,2,3,*] C. Spitaleri,[1,2] A. Mukhamedzhanov,[4] G. G. Rapisarda,[1,2] L. Campajola,[5] S. Cherubini,[1,2] V. Crucillá,[1,2] Z. Elekes,[7] Z. Fülöp,[7] L. Gialanella,[6] M. Gulino,[1,2] G. Gyürky,[7] G. Kiss,[7] M. La Cognata,[1,2] L. Lamia,[1,2] A. Ordine,[6] R. G. Pizzone,[1,2] S. Romano,[1,2] M. L. Sergi,[1,2] and E. Somorjai[7]

[1]*Laboratori Nazionali del Sud, INFN, Catania, Italy*

[2]*Dipartimento di Metodologie Fisiche e Chimiche per l'Ingegneria, Università di Catania, Catania, Italy*

[3]*Universitá Kore di Enna, Enna, Italy*

[4]*Cyclotron Institute, Texas A&M University, College Station, Texas, USA*

[5]*Dipartimento di Scienze Fisiche, Universitá Federico II, Napoli, Italy*

[6]*INFN, Sezione di Napoli, Italy*

[7]*ATOMKI, Debrecen, Hungary*

(Received 7 July 2008; revised manuscript received 26 September 2008; published 17 December 2008)

Two-proton scattering at sub-Coulomb energies has been measured indirectly via the Trojan horse method applied to the $p+d \rightarrow p+p+n$ reaction to investigate off-energy shell effects for scattering processes. The three-body experiment was performed at 5 and 4.7 MeV corresponding to a p-p relative energy ranging from 80 to 670 keV. The free p-p cross section exhibits a deep minimum right within this relative energy region due to Coulomb plus nuclear destructive interference. No minimum occurs instead in the Trojan horse p-p cross section, which was extracted by employing a simple plane-wave impulse approximation. A detailed formalism was developed to build up the expression of the theoretical half-off-shell p-p cross section. Its behavior agrees with the Trojan horse data and in turn formally fits the n-n, n-p, and nuclear p-p cross sections given the fact that in its expression the Coulomb amplitude is negligible with respect to the nuclear one. These results confirm the Trojan horse suppression of the Coulomb amplitude for scattering due to the off-shell character of the process.

DOI: 10.1103/PhysRevC.78.064001 PACS number(s): 25.45.De, 24.50.+g, 25.10.+s, 25.70.Hi

I. INTRODUCTION

The Trojan horse method (THM) [1–4] is a very powerful tool to study charged-particle reactions at sub-Coulomb energies because it makes it possible to extract their cross sections down to the relevant energies without experiencing Coulomb suppression. For this reason, it has been successfully applied to rearrangement reactions of astrophysical interest for the past 20 years [3,5–8]. In this article, we investigate the suppression of the Coulomb amplitude when the THM is applied to scattering processes. This is done by considering p-p scattering at low energy whose features, described below, can provide this important test for the THM.

p-p scattering represents one of the oldest source of quantitative information about the nuclear force [9,10]. Despite its simplicity, this was the first scattering between identical particles to be regarded as an exception, because distinct differences from pure quantum mechanical Mott scattering were observed. Indeed, in the description of such an interaction both Coulomb scattering and nuclear effects have to be considered. The Coulomb scattering is coherent with the nuclear one and interference terms between the two effects are expected to contribute to the cross section. In particular, there is a region at low proton-proton relative energy (E_{pp}) where the nuclear scattering amplitude in the ^{1}S state and the $l = 0$ partial wave of the Coulomb scattering amplitude give destructive interference. This interference generates the deep minimum in the p-p cross section (about 1 mbarn/sr) at $E_{pp} = 191.2$ keV and $\theta_{\mathrm{c.m.}} = 90^\circ$ [11], which is absent in the n-n and p-n scattering cross sections. A simple analytic expression of the p-p cross section at 90°, which accounts for the Coulomb scattering in all orbital angular momentum states plus nuclear scattering in the singlet S state, is given by [10]:

$$\sigma_{\mathrm{c.m.}}(90^\circ) = \left(\frac{2e^2}{m v_p^2}\right)^2 \left(1 - 2\frac{\sin\delta_0 \cos\epsilon}{\eta} + \frac{\sin^2\delta_0}{\eta^2}\right), \qquad (1)$$

where δ_0 is the phase shift generated by the nuclear field and η is the Coulomb parameter; $\epsilon = \delta_0 - \eta \ln 2$ is chosen in such a way that close to the minimum, where $\sin\delta_0 \approx \eta \approx 0.25$ rad, $\cos\epsilon \approx 1$; v_p is the laboratory velocity of the incoming proton, m its mass, and e its charge.

At low energy the p-p cross section is dominated by the first term (Coulomb term) of Eq. (1) that goes as $1/E^2$ (with E proton beam energy), whereas its second term describes the interference pattern. As the energy increases, the phase shift δ_0 increases while the Coulomb parameter η decreases. This makes the nuclear field dominating at higher energy and the p-p cross section is given essentially by the third term of Eq. (1), which drops as $1/E$.

If one considers that a nonsizable Coulomb amplitude would make the minimum to disappear, the strong interference pattern offers a unique possibility to validate the THM suppression of Coulomb amplitude for scattering. This has been realized by measuring the p-p elastic scattering within the region of the minimum through the ^{2}H(p, pp)n reaction in the quasi-free (QF) kinematics regime [12]. The idea is to check whether there is remaining evidence of the nuclear

*tumino@lns.infn.it

plus Coulomb interference minimum in the p-p cross section extracted via the THM.

The low-energy ^{2}H(p, pp)n reaction in QF kinematics was measured several times before (see Ref. [13] and references therein) but not in the region where the p-p Coulomb-nuclear interference takes place. The first measurements of this reaction at 6 MeV of beam energy in the interference area have been reported in Refs. [14,15]. The experimental setups provided the coincidence detection of the two exit protons as described in Refs. [14,15] giving values of E_{pp} down to 200 keV. Although experimental data seem to exclude the presence of the interference minimum, they have been considered as preliminary because it was not possible from those experiments to cover all the relevant relative energy region. In addition, only few couples of coincidence proton laboratory angles were contributing in QF kinematics to p-p center-of-mass (c.m.) values close to 90°.

To validate this result and reach lower p-p relative energies, the ^{2}H(p, pp)n experiment was performed at lower beam energies with dedicated setups. The present article reports on these experimental investigations. To extract the p-p cross section we apply the plane-wave impulse approximation (PWIA) [16], which leads to a factorized form of the TH double cross section. We will stress that the cross section for the binary reaction extracted from the THM is half-off-energy-shell (HOES), due to the virtual nature of the transferred particle. Here we will take into account the off-shell character of the transferred proton by performing a HOES calculation. This feature turns out to be very important below the Coulomb barrier while it gives negligible contribution at higher energies.

We will employ three steps in the evaluation of the experimental $p + p + n$ data:

(i) first the QF contribution to the three-body breakup reaction is selected from the experimental data after removing a small contribution due to the final-state interaction (FSI) [13] between the neutron and any one of the two protons;

(ii) compare the QF yield with the results of Monte Carlo simulations performed under the assumption of a pure quasi-free mechanism; the two-body cross section entering the PWIA factorization in the Monte Carlo simulations is given in turn by the on-energy-shell (OES) total p-p, n-n, n-p, and nuclear p-p cross sections from the literature [10] as well as by the calculated HOES p-p one;

(iii) finally, following the PWIA approach the cross section for the elastic p-p scattering is extracted from the QF data and compared with the calculated HOES one as well as with the OES counterparts in the energy region where the Coulomb-nuclear interference occurs.

II. THEORY OF THE TROJAN HORSE METHOD

The THM is an indirect technique for studying charged particle two-body reactions at sub-Coulomb energies (see Refs. [1–4] and references therein). The idea is to use nuclear clusters as virtual projectiles/targets to measure cross sections at ultra-low energies overcoming the main problems of direct measurements. As mentioned, this technique was successfully applied to nuclear astrophysics [3,5–8]. Indeed, when dealing with charged-particle reactions at astrophysical energies, the Coulomb barrier, usually of the order of few MeV, is much higher than the energies of interest ($\leqslant$100 keV), thus implying that the reaction takes place via a tunneling effect with an exponential decrease of the cross section, $\sigma(E) \sim \exp(-2\pi\eta)$. In addition, the screening effect of the nuclear charges due to the electron clouds surrounding the interacting nuclei leads to a higher cross section compared to the one in the case of bare nuclei [17,18] that represents the relevant parameter for astrophysics. Up to date, the only way to determine the bare nucleus cross section is by extrapolating the behavior of the higher energy data. The extrapolation is done in terms of the astrophysical S(E)-factor, which essentially removes the dominant energy dependence of the cross section due to the Coulomb barrier factor. The THM offers a novel approach to avoid the extrapolation providing the only existing way to measure the bare nucleus astrophysical S(E)-factor down to sub-Coulomb energies.

A. The Trojan Horse method and the quasi-free kinematics regime

The THM replaces the sub-Coulomb binary reaction:

$$A + x \rightarrow C + c. \tag{2}$$

by a suitable $2 \rightarrow 3$ particle process

$$A + a \rightarrow C + c + s, \tag{3}$$

establishing a relation between the two reactions by means of nuclear reaction theory. The latter is chosen in such a way that the target a (or equivalently the projectile) has a wave function with a large amplitude for the $x \oplus s$ cluster configuration, x being the target/projectile of the two-body reaction. In the application of the THM, we are interested in the process that can be regarded as a transfer reaction to the continuum, where the TH nucleus a breaks up into the nucleus x, which is transferred, and the nucleus s that remains as a spectator to the subreaction (2). In the three-body phase space, where this direct reaction mechanism gives the main contribution to the cross section, the momentum transfer to the spectator s is small. This is what we call the QF kinematics regime. The transferred nucleus appears only as a virtual particle in the reaction process, thus energy and momentum of the nucleus x do not obey the usual energy-momentum relation for a free particle.

Because the $A + a$ interaction occurs at an energy above the Coulomb barrier, the TH nucleus a breaks up inside the nuclear region of A without experiencing either Coulomb suppression or electron screening effects. Nevertheless, the quasi-free $A + x$ process can take place at sub-Coulomb, even negative, relative energy E_{Ax}, thanks to the key role of the $a = (sx)$ binding energy B_{sx} in compensating for the $A + a$ relative motion. This is clearly seen invoking energy and momentum conservation rules:

$$E_{Ax} = \frac{p_{Ax}^2}{2\,\mu_{Ax}} - \frac{p_{sx}^2}{2\,\mu_{sx}} - B_{sx}, \tag{4}$$

where $\mathbf{p}_{ij}$ is the relative momentum of particles i and j, $m_{ij} = m_i\, m_j/(m_i + m_j)$ is their reduced mass, and m_i is the mass of particle i. We note that $p_{Ax} \neq \sqrt{2\,\mu_{Ax}\, E_{\rm QF}}$ due to the virtual nature of particle x. In the QF kinematics $p_{sx} = 0$ and

$$E_{Ax} = E_{\rm QF} = \frac{p_{Ax}^2}{2\,\mu_{Ax}} - B_{sx}. \tag{5}$$

In the laboratory system (the target is at rest, which means $p_a = 0$ and $p_s = 0$):

$$\mathbf{p}_{Ax} = \frac{m_x\,\mathbf{p}_A - m_A\,\mathbf{p}_x}{m_x + m_A} = \frac{m_x}{m_x + m_A}\,\mathbf{p}_A, \tag{6}$$

where $\mathbf{p}_A$ is the momentum of projectile A. Then, from Eqs. (5) and (6) we get

$$E_{\rm QF} = \frac{m_x}{m_x + m_A}\,E_A - B_{sx}. \tag{7}$$

Both Eqs. (5) and (7) show how the binary reaction can be induced at very low $E_{\rm QF}$ in the THM using the beam energy E_A above the Coulomb barrier, a condition that is impossible to achieve in direct measurements due to the Coulomb barrier. It is important to notice that $E_{\rm QF}$ is uniquely determined from Eq. (7) once the projectile energy is fixed. Hence, determining the energy dependence of the binary reaction cross section from the THM requires changing the beam energy. From a practical point of view it is more convenient to fix the beam energy and deviate slightly from the optimal QF condition by allowing the relative momentum p_{sx} to vary in the interval $0 \leqslant p_{sx} \leqslant p_{sx}^{(\max)} < \kappa_{sx}$, where $\kappa_{sx} = \sqrt{2\,\mu_{sx}\,B_{sx}}$ is the $a = (sx)$ bound-state wave number. Thus, thanks to the Fermi motion of s and x inside a, it is possible to span the entire astrophysical energy region fixed by the cutoff, $\Delta p_{sx} = p_{sx}^{(\max)}$, in the p_{sx} momentum distribution. Usually the cutoff is of the order of a few tens of MeV/c performed on the p_s variable, the momentum of the spectator (in the laboratory system $\mathbf{p}_{sx} = \mathbf{p}_s = -\mathbf{p}_x$). This approach strongly deviates from the original idea [1] where, to reach the low energy region for the binary reaction, the initial velocity of the projectile A is compensated for by the Fermi motion of particle x. In this framework, a momentum of the order of hundreds of MeV/c is needed. This is very critical in the case of a TH nucleus with a predominant $l = 0$ intercluster motion, because such momenta populate the tail of the momentum distribution for particle x, making the separation from eventual background reaction mechanisms (like sequential decays feeding the same exit channel) very complicated. Moreover, the description of the tail is very sensitive to the theoretical approach applied to get the relevant binary reaction cross section, in contrast to the full shape at small p_s values, thus implying much more sophisticated treatments. In addition, higher relative momenta mean shorter intercluster distances and the role of particles as spectator is no longer so clearly defined. The novel approach makes it possible to overcome these problems in the extraction of the binary cross section.

B. Impulse approximation and half-off-shell effects

Let us consider the $A + a \to A + c + s$ breakup reaction in the three-body model with $a = (sx)$ and $A = C, s$, and $x = c$ constituent structureless particles. The exact reaction amplitude in the prior form is then given by

$$M^{(\rm prior)}(\mathbf{k}_{Cc}, \mathbf{k}_{Aa}) = \left\langle \Psi_f^{(-)} \middle| V_{Aa} \middle| \varphi_a\, \chi_{Aa}^{(0)} \right\rangle. \tag{8}$$

Here, $\Psi_f^{(-)}$ is the exact final state three-body scattering wave function with the incident wave corresponding to the $A + s + x$ three-body channel in the continuum, $V_{Aa} = V_{Ax} + V_{As}$, V_{ij} is the interaction potential between nuclei i and j, $\chi_{Aa}^{(0)}$ is the plane wave describing the relative motion of the noninteracting nuclei A and a in the initial state moving with the relative momentum $\mathbf{k}_{Aa}$. Note that the Coulomb interaction of particles A and a in the initial state is assumed to be screened for a moment. Because the exact final-state wave function is unknown usually for heavier nuclei the DWBA is used, but it cannot be applied for the $p + d \to p + n + p$ reaction under consideration. A priori, the Fadeev equations are required to get the wave function $\Psi_f^{(-)}$. In the simplest approach linked to the QF kinematics one can replace $\Psi_f^{(-)}$ by the product $\chi_s^{(0)}\,\chi_{Cc}^{(-)}$, where $\chi_{Cc}^{(-)}$ is the scattering wave function of particles C and c in the final state. Essentially, this reflects the assumption that in the QF kinematics the interaction of the spectator with particles C and c is reduced. Such an approximation represents the so-called PWIA [16,19–29], in which only the scattering of the fragments C and c in the final state is taken into account. It has been used to derive the low-energy two-body cross section in terms of the TH reaction (3) in the QF kinematics regime. This application is strengthened by previous investigative works at low energies [22,24,28–39].

The original expression for the PWIA (8) can be rewritten as the sum of the amplitude of the pole diagram (it contains the interaction potential V_{Ax}) and the one of the triangular diagram (containing the interaction potential V_{As}) [40]. If $s = n$, as in the case under consideration, then the spectator s interacts with the other particles only via nuclear interaction that we neglect in the QF conditions, i.e., approximate $V_{Aa} \approx V_{Ax}$. Then, the prior form amplitude for the QF breakup in the PWIA reduces to the amplitude of the pole diagram

$$M^{(\rm pole)}(\mathbf{k}_{Cc}, \mathbf{k}_{Aa}) = \left\langle \chi_s^{(0)}\,\chi_{Ax}^{(-)} \middle| V_{Ax} \middle| \varphi_a\,\chi_{Aa}^{(0)} \right\rangle. \tag{9}$$

Thus the pole amplitude is the PWIA for the relative motion $A + a$ in the initial state and for the relative motion of s and the center-of-mass of the system $A + x$, but the one of $A + x$ is taken accurately into account. For the QF $p + d \to p + p + n$ breakup reaction of interest, the pole diagram is shown in Fig. 1. In particular, the deuteron $a = d$ is the TH nucleus,

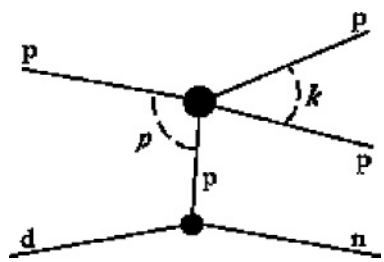

FIG. 1. Pole diagram describing the QF $p + d \to p + p + n$ process.

the neutron s is the spectator, and the proton $x = p$ is the transferred virtual particle.

The amplitude (9) of the pole diagram describing the TH reaction (3) consists of two factors. If we write down the integral in its matrix element (9) in the momentum representation, the two factors are given by

$$T(\mathbf{p}_{Ax}, \mathbf{k}_{Ax}) \sim \langle e^{i\,\mathbf{p}_{Ax}\cdot\mathbf{r}} \,|\, V_{Ax}(r)\, \chi^{(+)}_{Ax}(\mathrm{r})\rangle \tag{10}$$

representing the HOES p-p scattering amplitude, with $\chi^{(-)}_{Ax}(\mathrm{r}) \equiv \chi^{(-)}_{\mathbf{k}_{Ax}}(\mathrm{r})$, and

$$\varphi_a(p_{sx}) = \frac{W_a(p_{sx})}{p^2_{sx} + \kappa^2_{sx}}, \tag{11}$$

giving the Fourier transform of the (sx) bound-state wave function, with $W_a(p_{sx})$ amplitude of the virtual breakup $a \to s + x$, presently $d \to n + p$. For the case under consideration, $a = d$, the Hulthén wave function is a good approximation for $\varphi_a(p_{sx})$.

In a rigorous approach, the interaction between the nuclei in the initial and final channels should be taken into account [41]. However, if we are interested only in the energy dependence of the cross section, the treatment above is very well suited. Then the expression of cross section for the TH reaction (3) becomes particularly simple in the PWIA, being factorized into two terms corresponding to the pole mechanism shown in Fig. 1 [16,23,25–29]:

$$\frac{d^3\sigma}{dE_c d\Omega_c d\Omega_C} \propto [KF\ |\varphi_a(p_{sx})|^2] \left(\frac{d\sigma}{d\Omega_{\mathrm{c.m.}}}\right)^{\mathrm{HOES}}. \tag{12}$$

Here KF is a kinematical factor containing the final-state phase-space factor, which is a function of the masses, momenta, and angles of the outgoing particles

$$KF = \frac{\mu_{Aa}\, m_c}{(2\pi)^5 \hbar^7} \frac{p_C\, p_c^3}{p_{Aa}} \left[\left(\frac{\mathbf{p}_{Fs}}{\mu_{Fs}} - \frac{\mathbf{p}_{Cc}}{m_c}\right) \cdot \frac{\mathbf{p}_c}{p_c}\right]^{-1}; \tag{13}$$

Ω_j is the solid angle of particle j, $(F = A + x = c + C)$; $[(d\sigma/d\Omega)_{\mathrm{c.m.}}]^{\mathrm{HOES}}$ is the HOES differential cross section for the binary reaction (2) (here the p-p scattering), built up from Eq. (10) at the relative $x - A$ kinetic energy E_{QF} given by

$$E_{\mathrm{QF}} = E_{cC} - Q_2\,. \tag{14}$$

Here, Q_2 is the Q value of the binary reaction (2), which is zero for elastic scattering, and E_{cC} is the relative energy of the outgoing particles c and C ($E_{cC} = E_{pp}$ in our case).

Because $|\varphi_a(p_{sx})|^2$ is known from nuclear clustering studies, the product $KF\,|\varphi_a(p_{sx})|^2$ can be calculated, either analytically (for fixed angles) or via a Monte Carlo simulation. Therefore, it is possible to derive $[(d\sigma/d\Omega)_{\mathrm{c.m.}}]^{\mathrm{HOES}}$ from a measurement of $d^3\sigma/dE_c d\Omega_c d\Omega_C$ by using the following equation

$$\left(\frac{d\sigma}{d\Omega_{\mathrm{c.m.}}}\right)^{\mathrm{HOES}} \propto \left[\frac{d^3\sigma}{dE_c d\Omega_c d\Omega_C}\right] \frac{1}{KF|\varphi_a(p_{sx})|^2}. \tag{15}$$

It was demonstrated [41] that, due to the virtual character of fragment x (initially it is in the bound state of a), the Gamow factor does not appear in the initial $A + x$ state of the binary subprocess making it possible to extract its cross section down to the relevant energies without experiencing Coulomb suppression. This appears to be the only consequence of the off-energy-shell effects as suggested by the agreement between HOES and OES cross sections for the neutron induced ^{6}Li$(n, \alpha)^3$H reaction [42]. Thus, above the Coulomb barrier HOES and OES fully agree. This allows us to derive the absolute magnitude of the binary reaction cross section from a scaling to the OES data available at higher energies.

We note that in the case of elastic scattering, the off-shell suppression mechanism of the Coulomb interaction is quite different from that of rearrangement reactions. In particular, in the case of elastic scattering the total amplitude is given by the sum of the Coulomb and Coulomb-modified nuclear parts. As we will show, the off-shell effects cause the Coulomb amplitude to be suppressed compared to the nuclear part.

The PWIA has been successfully applied to determine the energy dependence of the triple differential cross section at E_{pp} higher than the Coulomb-nuclear interference minimum [13]. In this work, we extend the PWIA to the lower energies within the interference region. We underscore again that such a procedure will allow us to determine only the energy dependence of the HOES p-p cross section but not its absolute value. To check the applicability of the PWIA, the extracted energy dependence of the $p + p$ cross section will be compared with the calculations.

C. Half-off-shell theoretical p-p cross section

The Coulomb-modified nuclear HOES p-p scattering amplitude at low energies can be written in analytical form by adopting a separable s-wave Yamaguchi potential of the first rank [43]:

$$\begin{aligned} T^{\mathrm{CN}}(k, p) = {} & \sqrt{\frac{2}{\pi}} \frac{1}{k^2 + \beta^2} [B(k, p)]^{-i\eta} e^{-\pi\eta/2} \Gamma(1 + i\eta) \\ & \times \left(\sqrt{\frac{2}{\pi}} \frac{1}{p^2 + \beta^2} - \sqrt{\frac{2}{\pi}} \frac{1}{k^2 + \beta^2} \frac{k}{p} \right. \\ & \times \{ {}_1F_1[1,\ i\eta,\ 1 + i\eta,\ B_1(k, p)] \\ & \left. - {}_1F_1[1,\ i\eta,\ 1 + i\eta,\ B_0(k, p)] \} \right) \\ & \times \frac{1}{\lambda^{-1} + G_0(k, p)}. \end{aligned} \tag{16}$$

Here, $p \equiv p_{Ax}$ is the relative virtual p-p momentum in the entry channel of the p-p scattering (one of the protons is virtual) and $k \equiv p_{Cc}$ is the relative on-shell momentum of the outgoing protons. Paramaters $\beta = 1.095$ fm^{-1} and $\lambda = 2.4$ fm^{-3} were chosen to fit the low-energy p-p s-wave scattering phase shift [43]. η is the p-p Coulomb parameter in the exit channel and ${}_1F_1$ is the hypergeometric function,

$$\begin{aligned} G_0(k, p) = {} & \frac{1}{2\,\beta\,(\beta - i\,k)^2\,(1 + i\,\eta)} \\ & \times {}_1F_1[1,\ i\eta,\ 2 + i\eta,\ B_2(k)], \end{aligned} \tag{17}$$

$$B(k) = \frac{\beta + ik}{\beta - ik}, \tag{18}$$

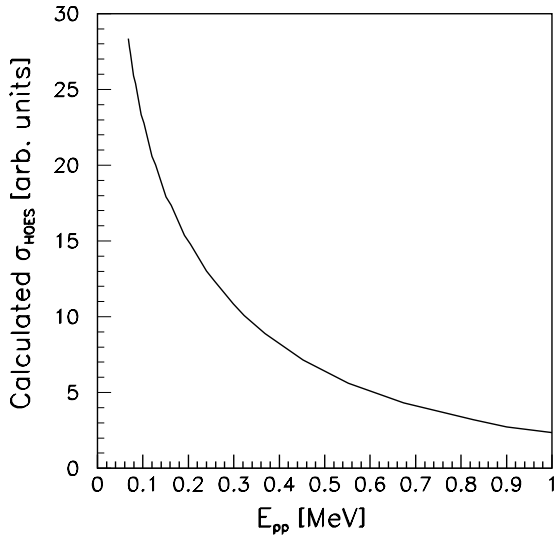

FIG. 2. Theoretical HOES p-p scattering cross section from Eq. (22).

$$B_1(k, p) = B(k)\frac{p-k}{p+k}, \tag{19}$$

$$B_0(k, p) = B(k)\frac{p+k}{p-k}, \tag{20}$$

$$B_2(k) = B(k)^2. \tag{21}$$

The HOES differential cross section for the low-energy p-p scattering is given by

$$\begin{aligned}\left(\frac{d\sigma}{d\Omega_{\text{c.m.}}}\right)^{\text{HOES}} &= \frac{1}{k^2}\left(\frac{1}{4}\left[\left|2\mu_{pp}\, e^2\, e^{-\pi\eta}\Gamma(1+i\eta)\right.\right.\right.\\ &\times\left.\left(\frac{(p^2-k^2)^{i\eta}}{(\mathbf{p}-\mathbf{k})^{2(1+i\eta)}}+\frac{(p^2-k^2)^{i\eta}}{(\mathbf{p}+\mathbf{k})^{2(1+i\eta)}}\right)-2\,T_{CN}(k,p)\right|^2\Big]\\ &+\frac{3}{4}\left[\left|2\mu_{pp}\, e^2\, e^{-\pi\eta}\Gamma(1+i\eta)\right.\right.\\ &\times\left.\left.\left(\frac{(p^2-k^2)^{i\eta}}{(\mathbf{p}-\mathbf{k})^{2(1+i\eta)}}-\frac{(p^2-k^2)^{i\eta}}{(\mathbf{p}+\mathbf{k})^{2(1+i\eta)}}\right)\right|^2\right]\Big).\end{aligned} \tag{22}$$

The part other than T_{CN} is the HOES Coulomb amplitude, with μ_{pp} the reduced mass of the two protons, and e the proton charge. The cross section in the first brackets corresponds to a total spin of the two protons $S = 0$ and contains even partial waves; at low energies $\text{T}_{\text{CN}}(k, p)$ contributes only to the s partial wave. The cross section in the second brackets corresponds to a total spin $S = 1$ and contains only odd partial waves.

We note that the HOES cross section depends on three independent invariants, the initial off-shell relative momentum of the two protons p, the OES exit relative momentum k, and the scattering angle, in contrast to two independent invariants, k and scattering angle, for the OES cross section. In the QF kinematics the off-shell momentum p is fixed and always larger than k (this feature will be later recalled), what constitutes a very important difference compared to the OES case where the entry momentum coincides with the exit one k. The $1/k^2$ geometrical factor in Eq. (22), makes the energy behavior of the HOES cross section comparable with the OES counterpart after normalization to it at higher energies. In contrast to the OES case, this factor must be introduced in the expression of the HOES cross section, due to the virtual nature of the process. The resulting HOES curve progress is shown in Fig. 2 as solid line. A drastic suppression of the Coulomb interaction is apparent even if we have multiplied the HOES cross section by the missing factor $1/k^2$. This is the key point that will be further discussed after showing the comparison with the OES cross section and the experimental HOES data.

III. THE EXPERIMENTS

The $^2\text{H}(p, pp)n$ experiment was performed at the ATOMKI, Debrecen (Hungary). A 5-MeV proton beam was delivered by the cyclotron accelerator with a beam energy spread of 10^{-3} onto a deuterated polyethylene target (98% of ^{2}H), 200 $\mu g/\text{cm}^2$ thick, placed at 90° with respect to the beam direction. The spot size of the beam on target was approximately 1 mm. Proton-proton coincidences were measured by four 500-μ-thick position sensitive detectors (PSD), each of them with an effective area of 5×1 cm^2. Some details concerning the working principle of such detectors are given soon after the description of the experiments. A schematic diagram of the experimental setup with the four PSDs is shown in the upper part of Fig. 3. Two of them were placed almost symmetrically with respect to the beam direction, covering angles 5° to 19° and 9° to 19°. On the same side of the less forward detector, the other two PSDs were centered at 29° and 59°, covering also 10°. The alignment of the detectors was checked by an optical system.

The trigger for the event acquisition was given by the coincidences between the most forward PSD (drawn with green color in Fig. 3), placed alone on one side of the scattering chamber, and any one of the three PSD's placed on the other side with respect to the beam direction (drawn with red color in Fig. 3). This setup allowed us to investigate the E_{pp} range from 550 keV down to 80 keV, right within the characteristic interference minimum in the direct p-p cross section, and a p-p center-of-mass angle $\theta_{\text{c.m.}} = 30°$ to 150°. This range corresponds to momentum values p_s of the undetected neutron up to 60 MeV/c, which fulfill the QF condition. This assures that the bulk of the QF contributions for the break-up process of interest falls inside the investigated regions.

Another experiment within the E_{pp} interference region was performed at the Dipartimento di Scienze Fisiche dell'Universitá Federico II, Naples (Italy), to substantiate the Debrecen results and to add some points in the region right above the p-p Coulomb barrier (up to about 700 keV). This would allow us also to check the consistency of the HOES formalism in a wider range. A 4.7-MeV proton beam was delivered by the 3-MV Tandem accelerator with a spot size of about 1 mm onto a deuterated polyethylene target, 200 μg/cm^2 thick, placed at 90° with respect to the beam direction. Two

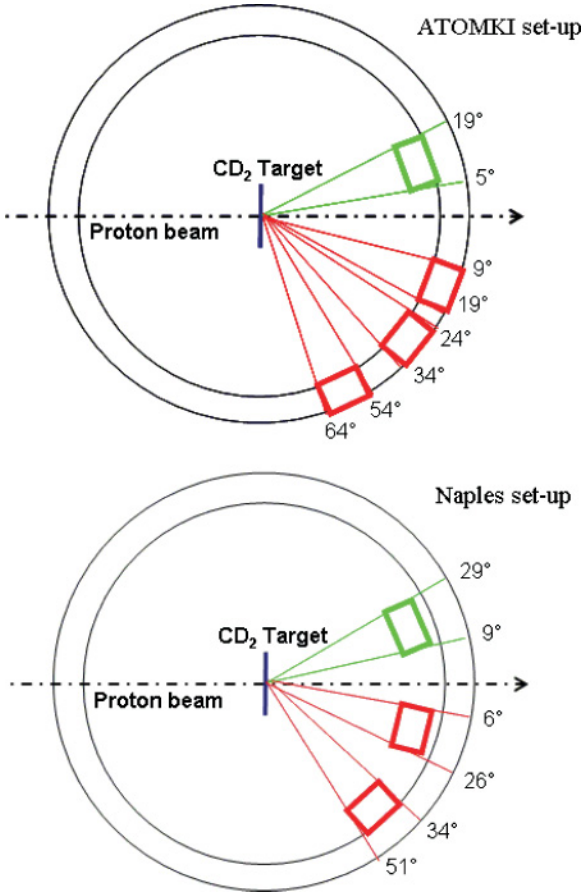

FIG. 3. (Color online) Schematic description of the experimental setups for the two experiments. Green and red colors help to visualize the coincidences between the detectors building up the trigger to the acquisition (see text for details).

proton coincidences were measured by three PSDs (see the lower part of Fig. 3 for a schematic view of this setup), two of them placed almost symmetrically with respect to the beam direction and covering the angular ranges 9° to 29° and 6° to 26°. The third PSD was placed on the same side of the most forward detector, covering angles 34° to 51°. Coincidences were registered between the 9° to 29° PSD (green color in the lower part of Fig. 3) and any one of the two PSDs placed on the other side with respect to the beam direction (drawn with red color in the lower part of Fig. 3).

A similar range as before was covered in terms of p-p center-of-mass angles, with a strong contribution in the region close to $\theta_{\text{c.m.}} = 90°$. In both experiments, energy and position signals for the detected particles were processed by standard electronics together with the delay between the time signals for each coincidence event and sent to the acquisition system for on-line monitoring and data storage for off-line processing.

A. Schematic description of a silicon PSD

A PSD is a quite popular detector providing the information on energy and angle of the detected particle. A schematic diagram of its layout is shown in Fig. 4. The detector is made

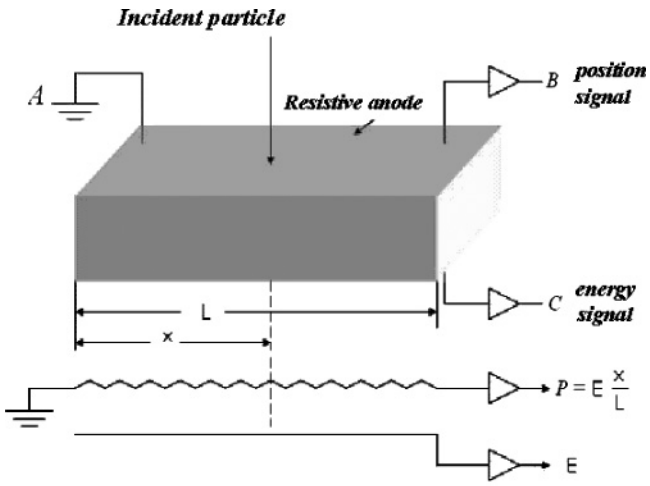

FIG. 4. Schematic description of a PSD layout.

of a standard single wafer of doped n-type silicon, which is depleted by a reverse voltage applied across the bulk of the crystal. As known, the energy released by the particle causes a charge signal (electrons/holes) at both faces. In the front face a p-type layer, usually created by boron implantation, acts as a resistive anode. At both ends of the implanted anode, two readout contacts allow one to deduce the position information from the partition of the energy signal. The collected charge divides into two fractions, each one in inverse proportion to the distance between the hit position of the particle and the strip-end collecting such a fraction.

Usually, the charge fraction is collected only from one of the two strip-ends (see Fig. 4), as this information is sufficient to reconstruct the position of the hitting particle. The other strip-end is closed through a resistor of the order of 1 kΩ (about a 20% of the total resistive layer), which ensures a measurable signal also when the hit position is close to this end. The intrinsic α resolution of a standard PSD is quoted as 300 μm for the position and about 0.5% for the energy.

IV. DATA ANALYSIS

A. Selection of the process

Energy and angle calibrations of the PSDs were performed using data acquired in preliminary runs of $p + {}^{197}\text{Au}$, $p + {}^{12}\text{C}$, $p + d$, and $p + p$ elastic scattering. Energy resolution was found to be better than 2%. During the preliminary runs, grids with equally spaced slits were placed in front of each PSD to establish a position-angle correspondence needed for the angle calibration. The angular resolution was found to be about 0.2°.

The kinematics were reconstructed under the assumption of a neutron as undetected particle. The corresponding locus of events in the E_p vs. E_p plane is shown in Fig. 5. In addition, if one considers a two-dimensional plot showing a kinematical variable, such as the energy or the angle of any one of the involved particles as a function of the Q value, coincidence events of interest should lie on a vertical line that cuts the Q-value axis at the expected value. The spectrum for the present case is reported in Fig. 6 where the laboratory angle of one

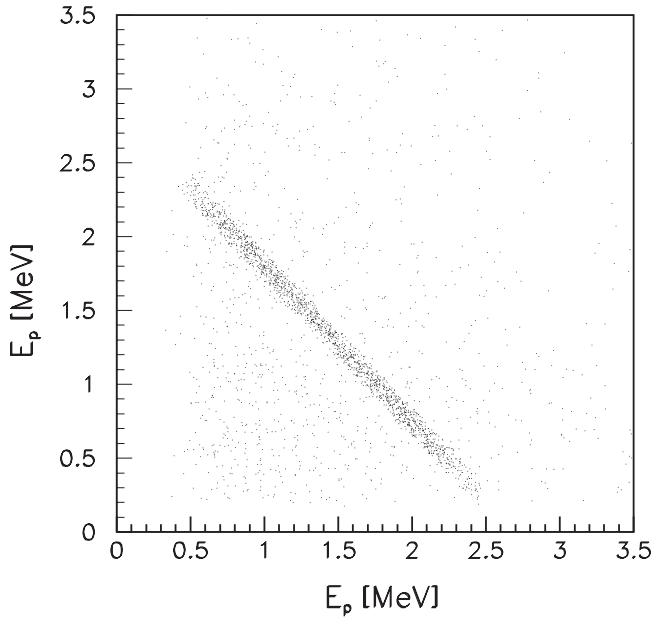

FIG. 5. Locus of events in the plane defined by the energies of the coincident particles E_p and E_p. The kinematical locus for the ^{2}H(p, pp)n reaction is apparent.

of the two detected protons (θ_p) is shown as a function of the Q value. A sharp vertical line shows up, crossing the Q-value axis at about -2.2 MeV. This value is in agreement with the expected one of -2.22 MeV, referring to the $p+p+n$ channel of interest. The resulting spectra, in particular the vertical Q-value line in Fig. 6, make us confident of the quality of the calibration and of the possibility to identify the $p+p+n$ channel.

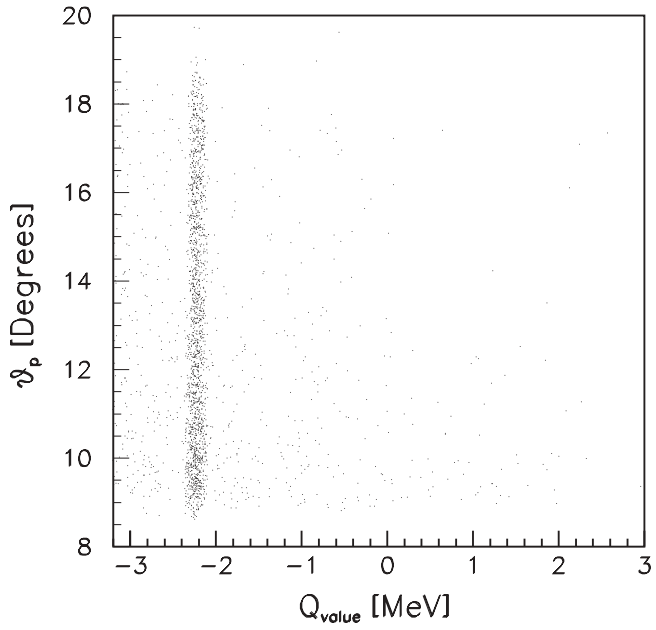

FIG. 6. Angle of one of the two detected protons θ_p vs. the Q_{value}.

B. Selection of the QF mechanism

The first step of the analysis is the selection of events corresponding to the ^{2}H(p, pp)n three-body reaction. This is accomplished by means of the graphical cut on the E_p vs. E_p kinematical locus shown in Fig. 5. To investigate the reaction mechanism involved, a calculation of the FSI between the neutron and any of the two protons was performed in the investigated E_{pp} region. In the present case, the n-p FSI is expected to contribute only slightly to the total cross section due to the low relative energy of the two protons. The effect of the FSI is usually taken into account by considering the s-wave matrix element given by

$$T_s = \frac{1}{D(E_{np})} T_S^0, \tag{23}$$

where $\mathrm{D}(E_{np})^{-1}$(E_{np} is the n-p relative energy) provides the so-called enhancement factor and T_S^0 is obtained by a simple modification of a standard Born approximation where the value of the wave function at the origin is considered [13,44,45]. In the effective range approximation, the n-p FSI enhancement factor is given by [44,45]

$$F_{np} = \frac{1}{|D(E_{np})|^2} = \frac{\left(k_{np}^2 + \alpha^2\right)^2 \frac{1}{4} r_0^2}{\left(-\frac{1}{a_{np}} + \frac{1}{2} r_0 k_{np}^2\right)^2 + k_{np}^2} \tag{24}$$

with

$$\alpha = \frac{1}{r_0}(1 + \sqrt{1 - 2r_0/a_{np}}), \tag{25}$$

where k_{np} is the relative momentum of the neutron and the proton; a_{np} is the n-p scattering length, and r_0 is the effective range. Because the n-p pair can be interacting either in the singlet or in the triplet state, both singlet and triplet enhancement factors have been used for considering the n-p FSI. The a_{np} and r_0 values entering the calculation were -23.748 fm and 2.75 fm for the singlet and 5.42 fm and 1.76 fm for the triplet factor.

The calculated n-p FSI yield projected onto the E_{pp} axis in the spanned energy interval experiences a quite flat energy dependence giving a contribution of less than 10% to the three-body coincidence yield, as shown in Fig. 7. This contribution was subtracted from the total events and a shape analysis of the experimental momentum distribution for the neutron was carried out with the remaining data. This is an observable that turns out to be very sensitive to the reaction mechanism. Dividing the quasi-free coincidence yield by the kinematic factor, we are left with a quantity that is proportional to the product of the momentum distribution for the neutron and the differential HOES p-p two-body cross section [see Eq. (12)], as given by:

$$|\varphi_a(p_s)|^2 \left(\frac{d\sigma}{d\Omega_{\text{c.m.}}}\right)_{E_0}^{\text{HOES}} \propto \left[\frac{d^3\sigma}{d\Omega_p d\Omega_p dE_{\text{c.m.}}}\right] [KF]^{-1}, \tag{26}$$

where E_0 is the mean energy of the E_{pp} relative energy window. In each restricted E_{pp} range, the differential binary cross section $(d\sigma/d\Omega_{\text{c.m.}})^{\text{HOES}}$ of the p-p scattering can be considered almost constant. Thus the experimental p_s momentum

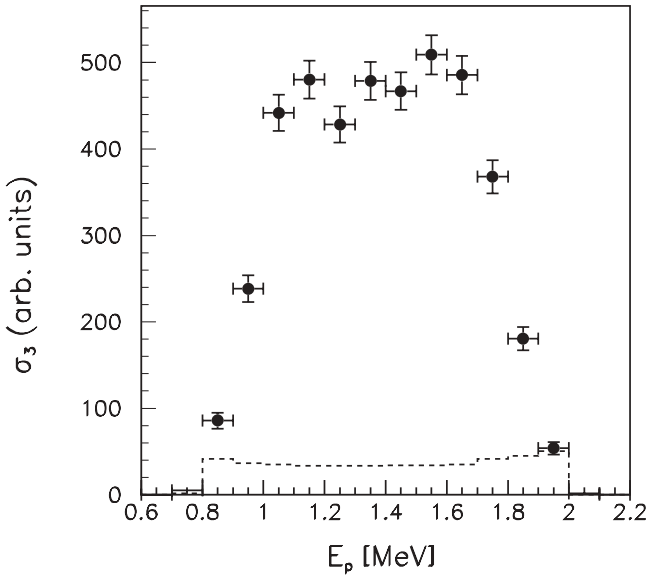

FIG. 7. Three-body coincidence yield σ_3 projected onto the proton energy axis E_p. The dashed line represents the contribution of the n-p FSI.

distribution is given by:

$$|\varphi_a(p_s)|^2 \propto \left[\frac{d^3\sigma}{d\Omega_p d\Omega_p dE_{\text{c.m.}}}\right][KF]^{-1} \ . \qquad (27)$$

This quantity was derived for the two experimental runs and it is shown in Fig. 8 as filled circles for the ATOMKI experiment and open ones for the Naples run. Its width (full width at half maximum, FWHM) of about 40 MeV/c in both cases is lower than the theoretical asymptotic value for the p-n system in the

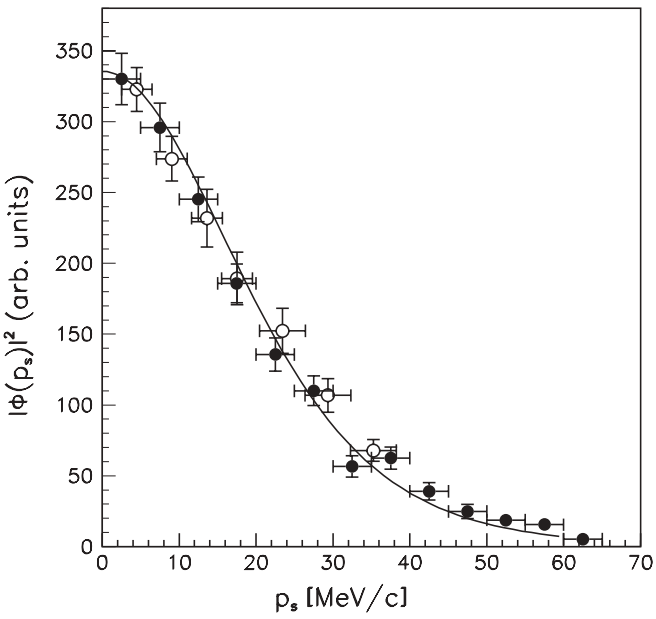

FIG. 8. Experimental neutron momentum distribution for the ATOMKI (full circles) and Naples runs (open circles). The dashed line represents the shape given by the square of the n-p Hulthén bound-state wave function in momentum space.

deuteron (58 MeV/c) obtained from the p-n bound-state wave function, in agreement with the one expected for the $p+d$ interaction at these beam energies [46]. This result, interpreted as due to distortion effects [46–48], is yet to be fully understood and three-body Faddeev equation calculations would be useful.

The full line superimposed onto the data in Fig. 8 is the theoretical shape given by the squared Fourier transform of the s-wave radial Hulthén function associated with the deuteron bound state:

$$\varphi_a(p_s) = \frac{1}{\pi}\sqrt{\frac{ab(a+b)}{(a-b)^2}}\left[\frac{1}{a^2+p_s^2} - \frac{1}{b^2+p_s^2}\right] \qquad (28)$$

with parameters $a = 0.2317$ fm^{-1} and $b = 0.3$ fm^{-1} [37] and normalization constant fixed at the experimental maximum. The b parameter has been changed from 1.202 fm^{-1}, corresponding to the asymptotic FWHM, to the present value to reproduce the experimental width.

We note that the Hulthén (pn) bound-state wave function is simultaneously the eigenfunction of both Hulthén and Yamaguchi separable potentials making the treatment of the (pn) bound state and the p-p scattering consistent. A quite fair agreement shows up, giving us confidence that in the experimentally selected kinematical region the QF mechanism gives the main contribution. For further data analysis, only events with p_s values lower than 20 MeV/c were considered, because they give contributions in the $\theta_{\text{c.m.}}$ region close to $90°(80° \leqslant \theta_{\text{c.m.}} \leqslant 100°)$.

V. RESULTS

A. The TH $p+d$ cross section

We note that a rigorous analysis of the experimental data requires the full three-body Faddeev calculations with the Coulomb p-p interaction [49]. However, it is impossible to extract the HOES p-p scattering amplitude from such calculations. As mentioned before, we employ a simple PWIA described by the pole diagram shown in Fig. 1. The amplitude of this diagram is proportional to the HOES p-p scattering amplitude, where one of the incoming protons is HOES while both exiting protons are OES.

The experiment was simulated by means of a Monte Carlo calculation based on the PWIA. The reaction was assumed to proceed through a pure quasi-free mechanism and all experimental constraints in energy and scattering angles for the detected particles were taken into account. The momentum distribution of the neutron inside the deuteron was described in terms of the parametrization given in Eq. (28). The HOES two-body cross section entering the calculation was first replaced with the free p-p one, where the $l = 0$ phase shift is calculated using the formalisms reported in Ref. [10] with scattering length $a_p = -7.806$ fm and effective radius $r_0 = 2.794$ fm. The three-body cross section was calculated for proton laboratory angles corresponding to p-p center-of-mass values close to 90° and compared with the experimental coincidence yield corrected for the geometric efficiency of the experimental setup. Results as a function of a proton laboratory energy E_p are reported in Fig. 9(a) for the ATOMKI experiment and (b) for the Naples one: the

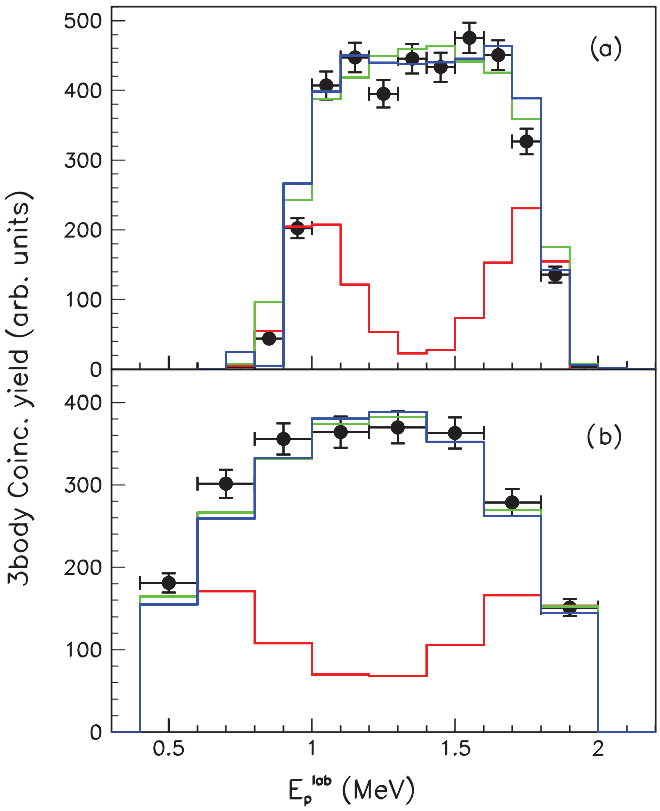

FIG. 9. (Color online) Experimental three-body cross section (filled circles) vs. proton laboratory energy E_p^{lab} from the Atomki (a) and the Naples runs (b). Solid lines represent: (red) the calculated OES p-p cross section; (green) the calculated nuclear p-p cross section; (blue) the calculated HOES p-p cross section.

three-body coincidence yield is given as filled circles, whereas the red solid line shows the calculation. A clear disagreement is apparent.

Then, another set of calculations was performed by introducing the on-shell n-n, n-p, and nuclear p-p ones [10]. The expression of the nuclear two-body cross section at low energy was considered for different values of the a and r_0 parameters: $a = -18.5$ fm, $r_0 = 2.75$ fm for the n-n, $a = 23.748$ fm, $r_0 = 2.75$ fm for the n-p, $a = -17.3$ fm, $r_0 = 2.85$ fm for the nuclear p-p scattering [50]. Results are reported also in Fig. 9(a) (ATOMKI) and (b) (Naples) as green solid lines. The calculations give practically the same energy behavior, which is represented by using the same solid line. It is clearly seen the agreement with experimental data.

When the HOES p-p cross section is used in Eq. (12), the calculation (solid line) nicely fits the experimental behavior of the coincidence yield as shown by the blue solid lines on the same Fig. 9(a) (ATOMKI) and (b) (Naples). One can clearly observe that the HOES cross section strongly resembles the behavior of n-n, n-p, or nuclear p-p cross section for the reason that will be further explained.

B. From the TH $p + d$ reaction to the HOES p-p scattering cross section

Following the PWIA approach [Eq. (15)], it is possible to derive the THM differential two-body cross section from the selected three-body coincidence yield divided by the $|\varphi_a(p_s)|^2 KF$ factor. The geometrical efficiency of the experimental setup as well as the detection thresholds were accounted for in the procedure. An error calculation for E_{pp} was also performed giving a value ranging from 15 to 20 keV the minimum estimate corresponding to the phase-space region where the magnifying glass effect is more efficient [51]. Essentially this effect works better if we are closer to the minimum of E_{pp} when reported as a function of the energy of one of the two protons, namely there is a weaker dependence of E_{pp} on it. The extracted p-p HOES cross section from both runs is presented in Fig. 10(a) as a function of E_{pp} in a wider E_{pp} range with respect to that reported in Ref. [12] (black dots for the 5-MeV run and green dots for the 4.7-MeV one) and compared to the free p-p cross section (black solid line) [10] with the same parameters as used before in the calculation of the three-body cross section [see Figs. 9(a) and 9(b)]. The red solid line represents the calculated HOES p-p cross section [Eq. (22)]. Both calculated curves are integrated over $80^\circ \leqslant \theta_{\text{c.m.}} \leqslant 100^\circ$ and averaged over an energy bin of

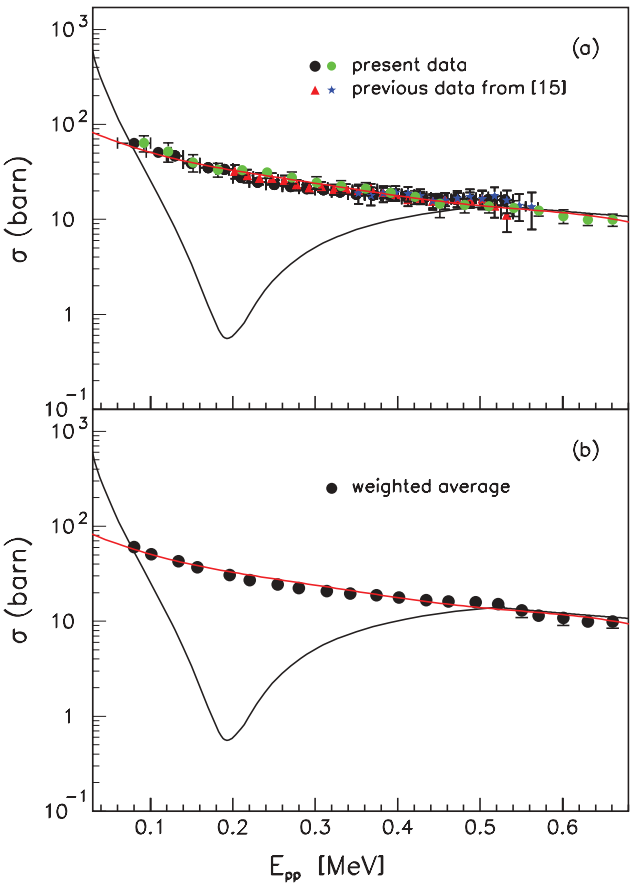

FIG. 10. (Color online) (a) THM two-body cross section (black and green dots from present experimental work, red triangles and blue stars from previous work [15]) vs. E_{pp}. Solid line represents the theoretical OES p-p cross section calculated as explained in the text. The red solid line is the HOES cross section calculated using Eq. (22). (b) Weighted average of all the experimental data shown in (a) vs. E_{pp} with the same meaning for the solid lines as above.

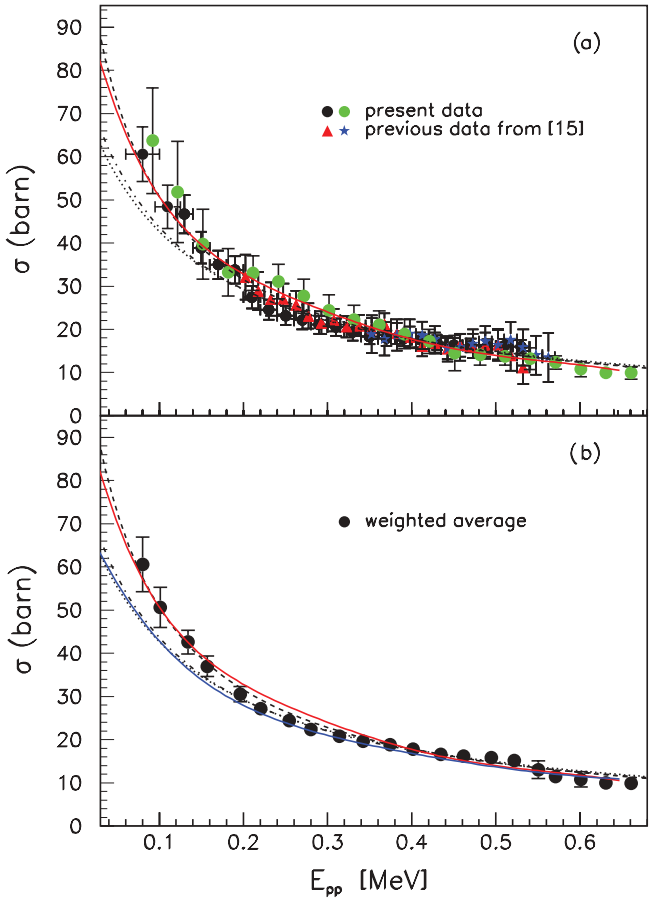

FIG. 11. (Color online) (a) THM two-body cross section (black and green dots from present experimental work, red triangles and blue stars from previous work [15]) vs. p-p relative energy E compared with the on-shell n-n (dashed-dotted line), p-n (dashed line), and pure nuclear p-p (dotted line) ones. The HOES calculated cross section is also reported as red solid line. (b) Weighted average of all the experimental data shown in (a) vs. E_{pp}. The blue solid line represents the theoretical HOES p-n cross section. The other lines have the same meaning as in (a).

20 keV. Experimental and calculated HOES cross sections are normalized to the calculated OES one at E_{pp} close to the Coulomb barrier (500 keV). Vertical error bars in the figure include statistical and normalization errors as well as the error due to the subtraction of the FSI contribution. Data from previous $p+d \rightarrow p+p+n$ experiments [15] are also shown as red triangles and blue stars. The weighted average of all sets of data is reported in Fig. 10(b) compared to the calculated curves as in Fig. 10(a). We observe a striking disagreement between the THM (HOES) and the free p-p (OES) cross sections throughout the region of the interference minimum. Indeed, the minimum is missing in the THM data that in contrast nicely fits the calculated HOES p-p cross section Eq. (22). However, one can see that right above the Coulomb barrier, in the region where the free p-p scattering is dominated by the nuclear field [10,13], both curves are in agreement with the additional THM points referring to the 4.7-MeV run.

The THM p-p cross section was further compared with the on-shell n-n, p-n, and pure nuclear p-p ones [10] with the same parameters [50] entering the PWIA parametrizations as before. Results are reported in Figs. 11(a) and 11(b) (weighted average of all the experimental points), with a dashed-dotted line for the n-n, dashed line for the p-n, and dotted line for the pure nuclear p-p cross section. The calculated HOES cross section is again shown for completeness (red solid line). Good agreement between the OES nucleon-nucleon nuclear cross sections and the THM data shows up.

In addition, one can obtain the energy dependence of the HOES n-n cross section simply replacing the two proton charges Ze by zero in the HOES theoretical formulas. The result is reported in Fig. 11(b) as a blue solid line. Surprisingly, it fairly reproduces the behavior of the n-n and pure nuclear p-p cross sections. This result is in agreement with the one reported in Ref. [42] because it excludes the existence of off-energy-shell effects when the Coulomb barrier is absent.

VI. DISCUSSION AND CONCLUSIONS

The results above represent compelling evidence of the validity of the THM method for elastic scattering: the experimental HOES p-p scattering cross section does not exhibit the interference minimum. Thus it strongly disagrees with the OES p-p behavior, heavily affected at low energies by the Coulomb interaction. They come to the agreement right above the Coulomb barrier where the OES p-p cross section is given essentially by the nuclear part; in contrast, the experimental HOES p-p scattering cross section has practically the same energy dependence as pure nuclear OES nucleon-nucleon cross sections throughout the whole E_{pp} range investigated; the experimental HOES p-p scattering cross section extracted from the TH reaction is very well reproduced by the calculated HOES p-p behavior. This indicates that the PWIA in the QF kinematics regime can be used to obtain the energy dependence of the p-p cross section even in the region where strong Coulomb-nuclear interference takes place for the OES p-p scattering. The behavior of the low-energy HOES cross section can be easily explained using Eq. (22). As already mentioned in the HOES scattering, the initial p and final k momenta are different by definition. In particular, for the $p+d \rightarrow p+p+n$ reaction in the QF kinematics ($p_s = 0$), $p^2 = k^2 + 2\,\mu\, B_{sx}$, where in the present case B_{sx} is the deuteron binding energy. That is why p is always larger than k. Hence the transfer momentum in the p-p elastic scattering $|\mathbf{p} - \mathbf{k}|$ at angles near 90° becomes large enough, compared to the OES case, to suppress the Coulomb HOES amplitude. For example, in the E_{pp} region where the OES cross section exhibits the interference minimum, $|\mathbf{p} - \mathbf{k}|$ is about of 0.3 fm^{-1}, making it possible to probe a distance between the two protons of the order of 3 fm, where the nuclear scattering dominates. In contrast, the corresponding transfer momentum in the on-shell p-p scattering is around 0.1 fm^{-1}, matching with a distance of about 10 fm, where only the Coulomb interaction is present.

The resulting HOES cross section at low energies is therefore dominated by the Coulomb modified nuclear amplitude

T_{CN}, revealing the typical behavior of the higher energy p-p cross section, far from the interference region. The Coulomb interaction does not affect the energy behavior of T_{CN} at least down to $E_{pp} \sim 200$ keV because the p-p Coulomb parameter is small. That is why the HOES cross section formally fits the OES nucleon-nucleon nuclear cross sections. However, at lower E_{pp} the HOES cross section slightly deviates from the OES nuclear p-p one and just accidentally appears better in agreement with the behavior of the n-p cross section. The n-p scattering is increasing more rapidly than the n-n and p-p counterparts when the energy goes to zero. This is because in the case of low-energy n-n and p-p nuclear scattering only the singlet state contributes, in contrast with the n-p scattering where both singlet and triplet states do. In particular, the behavior of the low-energy n-n and p-p nuclear cross sections are affected by the virtual singlet poles at -133 keV and $-140 - i467$ keV [52], whereas the low-energy n-p cross section is dominated by the deuteron pole at -2.224 MeV in the triplet state and by the virtual one at -66 keV in the singlet state.

Responsible for the little increase of the HOES cross section, which is contributed only by the singlet state, is the residual Coulomb interaction in T_{CN}. This consideration is strengthened by the apparent agreement between the HOES n-n cross section, free of any Coulomb effect, and both the OES n-n and nuclear p-p counterparts. However, the striking result is that the HOES p-p cross section is closely reproducing the behavior of the THM data within the entire E_{pp} range investigated.

In conclusion, through a mechanism that differs from that of nuclear rearrangement reactions, the present work strongly sustains the THM basic feature, namely the suppression of Coulomb effects in the two-body cross section at sub-Coulomb energies. This appears to be a universal effect whether we consider binary elastic or rearrangement processes. This result puts on firmer grounds the applicability of the THM in nuclear astrophysics as well as in all physics contexts where it can be important to investigate nuclear effects at low energies. Moreover, another issue has been readdressed with the agreement between the energy behavior of the HOES p-n cross section and that of the OES n-n and nuclear p-p ones, namely the lack of off-energy-shell effects other than the Coulomb suppression. It should be possible, for example, to extract the low-energy behavior of the n-n and n-p forces from the study of the QF $n + d \rightarrow n + n + p$ and $p + d \rightarrow p + n + p$ reactions, respectively.

However, other questions have to be answered when applying the THM. In particular, when dealing with the indirect study of light heavy-ion resonant reactions at sub-Coulomb energies [53,54], it is important to determine the contribution of the different partial waves to the OES and HOES cross sections. As known, direct measurements at lower energies are extremely difficult because of the high Coulomb barrier. Moreover, light heavy-ion reactions proceed through resonant structures even at low energies, due to the high level density in the excitation energy region of their compound nuclei. This complicates the extrapolation procedure from available data to very low energies. The THM offers a valid alternative path to obtain this information, but the angular distribution analysis of the fragments is needed to get the OES $S(E)$ factor from the THM data. For direct rearrangement reactions with large Q values, both OES and HOES cross sections have practically identical shapes because they are contributed dominantly by the s wave [4]. For the elastic Coulomb-modified nuclear scattering at sub-Coulomb energies, the fast decrease of the scattering phase shifts for $l > 0$ makes sure that only the s wave strongly contributes to the HOES and OES nuclear scattering cross sections. This is in agreement with the present results.

ACKNOWLEDGMENTS

The authors thank the technical staff of the Tandem accelerator at the Dipartimento di Scienze Fisiche dell'Universitá Federico II, Naples, for their valuable support during the experiment. They warmly acknowledge Professor R. E. Tribble for careful reading the manuscript and for the fruitful suggestions. This work was supported in part by OTKA T-049245, IN-64269, K68801, and the US DOE under Grant No. DE-FG02-93ER40773.

[1] G. Baur, Phys. Lett. **B178**, 135 (1986).
[2] S. Cherubini *et al.*, Astrophysical J. **457**, 855 (1996).
[3] C. Spitaleri *et al.*, Phys. Rev. C **69**, 055806 (2004).
[4] A. M. Mukhamedzhanov, C. Spitaleri, and R.E. Tribble, arXiv:nucl-th/0602001v1 (2006).
[5] C. Spitaleri *et al.*, Phys. Rev. C **63**, 005801 (2001).
[6] M. Lattuada *et al.*, Astrophysical J. **562**, 1076 (2001).
[7] A. Tumino *et al.*, Phys. Rev. C **67**, 065803 (2003).
[8] M. La Cognata *et al.*, Phys. Rev. C **72**, 065802 (2005).
[9] G. Breit, H. M. Thaxton, and L. Eisenbud, Phys. Rev. **55**, 1018 (1939).
[10] J. D. Jackson and J. M. Blatt, Rev. Mod. Phys. **22**, 77 (1950).
[11] H. Dombrowski *et al.*, Nucl. Phys. **A619**, 97 (1997).
[12] A. Tumino *et al.*, Phys. Rev. Lett. **98**, 252502 (2007).
[13] V. Valković *et al.*, Nucl. Phys. **A166**, 547 (1971).
[14] M. G. Pellegriti *et al.*, Prog. Theor. Phys. Suppl. **154**, 349 (2004).
[15] A. Tumino *et al.*, Nucl. Phys. **A787**, 337 (2007).
[16] G. Jacob and Th. A. Maris, Rev. Mod. Phys. **38**, 121 (1966).
[17] H. J. Assenbaum *et al.*, Z. Phys. A **327**, 461 (1987).
[18] F. Strieder *et al.*, Naturwissenschaften **88**, 461 (2001).
[19] G. F. Chew, Phys. Rev. **80**, 196 (1950).
[20] V. G. Neudatchin and Y. F. Smirnov, Atom. Energ. Rev. **3**, 157 (1965).
[21] P. G. Roos *et al.*, Phys. Rev. C **15**, 69 (1977).
[22] N. S. Chant and P. G. Roos, Phys. Rev. C **15**, 57 (1977).
[23] M. Jain *et al.*, Nucl. Phys. **A153**, 49 (1970).
[24] A. K. Jain *et al.*, Nucl. Phys. **A216**, 519 (1973).
[25] A. Guichard *et al.*, Phys. Rev. C **4**, 700 (1971).
[26] Đ. Miljanić *et al.*, Nucl. Phys. **A215**, 221 (1973).
[27] Đ. Miljanić *et al.*, Phys. Lett. **B50**, 330 (1974).
[28] J. Kasagi *et al.*, Nucl. Phys. **A239**, 233 (1975).
[29] I. Slaus *et al.*, Nucl. Phys. **A286**, 67 (1977).
[30] N. Arena *et al.*, Nuovo Cimento Soc. Ital. Fis., A **45**, 405 (1978).

[31] M. Lattuada *et al*., Nuovo Cimento Soc. Ital. Fis., A **62**, 165 (1981).
[32] M. Lattuada *et al*., Nuovo Cimento Soc. Ital. Fis., A **69**, 1 (1982).
[33] M. Lattuada *et al*., Nucl. Phys. **A458**, 493 (1986).
[34] M. Lattuada *et al*., Z. Phys. A **330**, 183 (1986).
[35] M. Zadro *et al*., Z. Phys. A **325**, 119 (1986).
[36] M. Zadro *et al*., Nucl. Phys. A **474**, 373 (1987).
[37] M. Zadro, D. Miljanic, C. Spitaleri, G. Calvi, M. Lattuada, and F. Riggi, Phys. Rev. C **40**, 181 (1989).
[38] S. Blagus *et al*., Z. Phys. A **337**, 297 (1990).
[39] G. Calvi, M. Lattuada, D. Miljanic, F. Riggi, C. Spitaleri, and M. Zadro, Phys. Rev. C **41**, 1848 (1990).
[40] I. S. Shapiro, *Proceedings of the XXXVIII International School of Physics "Enrico Fermi"* (Academic Press, New York/London, 1967), p. 210.
[41] A. M. Mukhamedzhanov *et al*., Eur. Phys. J. A **27**, 205 (2006).
[42] A. Tumino *et al*., Eur. Phys. J. A **27**, 243 (2005).
[43] H. van Haeringen and R. van Wageningen, J. Math. Phys. **16**, 1441 (1975).
[44] M. C. Goldberger and K. M. Watson, *Collision Theory* (Wiley, New York, 1964), p. 540.
[45] K. M. Watson, Phys. Rev. **88**, 1163 (1952).
[46] D. J. Margazioties *et al*., Phys. Rev. C **2**, 2050 (1970).
[47] S. Barbarino, M. Lattuada, F. Riggi, C. Spitaleri, and D. Vinciguerra, Phys. Rev. C **21**, 1104 (1980).
[48] R. G. Pizzone *et al*., Phys. Rev. C **71**, 058801 (2005).
[49] E. O. Alt and M. Rauh, Phys. Rev. C **49**, R2285 (1994).
[50] G. A. Miller *et al*., Phys. Rep. **194**, 1 (1990).
[51] G. Baur and H. Rebel, Annu. Rev. Nucl. Part. Sci. **46**, 321 (1996).
[52] L. P. Kok, Phys. Rev. Lett. **45**, 427 (1980).
[53] M. La Cognata *et al*., Phys. Rev. C **76**, 065804 (2007).
[54] M. L. Sergi *et al*., *OMEG07, the 10th International Symposium on Origin of Matter and Evolution of Galaxies: From the Dawn of Universe to the Formation of Solar System, AIP Conference proceedings*, **1016** (2008), p. 433.